Mobility of the Active Site Bound Paraoxon and Sarin in Zinc-Phosphotriesterase by Molecular Dynamics Simulation and Quantum Chemical Calculation

Jaroslav Koča, Chang-Guo Zhan, Robert C. Rittenhouse, and Rick L. Ornstein*

Contribution from the Pacific Northwest National Laboratory, Battelle-Northwest, Environmental Technology Division, Mailstop K2-21, Richland, Washington 99352

Received February 4, 2000

Abstract: The kinetic data published on phosphotriesterase (PTE), with various complexed metals, clearly indicates that the P═O and P═S bonds of phosphotriester and thiophosphotriester substrates, respectively, are strongly polarized by one or both of the active site complexed metal ions. However, this observation is not consistent with the three-dimensional X-ray crystal structure of zinc-substituted PTE with active site bound substrate analogue diethyl 4-methylbenzylphosphonate. In this structure, the distance between the phosphoryl oxygen and the nearest zinc is 3.4 Å, a distance too large to afford strong polarization. In the present paper, the geometry and mobility of various PTE active site−substrate complexes are examined by performing both molecular dynamics (MD) simulations and quantum mechanical calculations. Two known substrates are considered, paraoxon and sarin, although their turnover rates vary about 100-fold. The results indicate that PTE forms a complex with either substrate in which the phosphoryl oxygen becomes strongly coordinated with the less buried zinc atom. It is shown that the geometry of the active site is changed when the protein is immersed in a water bath and relaxed by MD. The most substantial conformational change is the opening of the gateway in a pocket where the location of the leaving group is expected. The opening is observed for the pure enzyme as well as for the enzyme/substrate complexes and it ranges from 11 to 18 Å. It is also shown that the pockets, in which the substrate substituents are localized, exhibit different flexibility and interact with the substrate with coordinated conformational adjustments.

Introduction

Phosphotriesterase (PTE) from *Pseudomonas diminuta* catalyzes the hydrolysis of organophosphorus pesticides and related nerve agents, i.e., acetylcholinesterase inhibitors, with surprisingly high turnover. The k_{cat} values for the best substrates, such as paraoxon (see Scheme 1), approach nearly 10^4 s^{-1} at 25 °C.[1]

There is much current interest in understanding the details of the catalytic mechanism. The questions discussed in the literature include the role of active site residues in the enzymatic reaction,[2] stereochemistry of the reaction,[3] and also the role of the metal ion in the active site structure and in the reaction mechanism.[4] Two high-resolution X-ray crystal structures are available: one for zinc-substituted[5] PTE complexed with the substrate analogue, diethyl 4-methylbenzylphosphonate, and one for cadmium-substituted[6] PTE. The geometry of the active site is somewhat different for each of them. In zinc-complexed PTE, the two metal ions in the active site are separated by 3.3 Å, while for cadmium-substituted PTE the Cd−Cd distance is 3.8 Å. It has also been shown[4] that the catalytic activity depends on the metal ion and thus differs for Zn- and Cd-substituted PTE. One of two bridging ligands of the binuclear metal center is a carbamylated Lys (residue 169), and the other bridging ligand is oxygen. Since hydrogen atoms cannot be determined by X-ray diffraction techniques, it is experimentally undetermined whether the bridging oxygen is in the form of water or hydroxide. Theoretical molecular dynamics and quantum mechanics studies[7] indicate that the bridging oxygen in zinc-substituted PTE exists in the form of hydroxide ion, OH^-.

The active site of PTE is composed of three pockets where the substituents on the central phosphorus atom are positioned[8] (Scheme 3). The present work lends further support to this characterization of the active site and indicates that also the Gly-60 residue, previously not considered in the literature, is an important part of pocket 2. It has been shown that this residue plays a role in the selectivity of the enzyme.[8]

Unfortunately, there are no X-ray crystal structures of PTE complexed with a true substrate. The experimental hydrolysis data show[9] that the bond cleavage step is rate limiting only when the pK_a of the leaving group is greater than 8, whereas the rate-limiting step involves a conformational change or diffusion-controlled dissociation when the pK_a is less than 8.

The experimental data also indicate that hydrolysis proceeds with a net inversion of stereochemistry at the phosphorus center.[3] This suggests an S_N2-type mechanism for which the attacking nucleophile (OH^- in this case) and the leaving group should

(1) Omburo, G. A.; Kuo, J. M.; Mullins, L. S.; Raushel, F. M. *J. Biol. Chem.* **1992**, *267*, 13278.
(2) Kuo, J. M.; Chae, M. Y.; Raushel, F. M. *Biochemistry* **1997**, *36*, 1982.
(3) Lewis, W. E.; Donarski, W. J.; Wild, J. R.; Raushel, F. M. *Biochemistry* **1988**, *27*, 1591.
(4) Hong, S.-B.; Raushel, F. M. *Biochemistry* **1996**, *35*, 10904.
(5) Vanhooke, J. L.; Benning, M. M.; Raushel, F. M.; Holden, H. M. *Biochemistry* **1996**, *35*, 6020.
(6) Benning, M. M.; Kuo, M. M.; Raushel, F. M.; Holden, H. M. *Biochemistry* **1995**, *34*, 7973.
(7) Zhan, C.-G.; Souza, O. N. d.; Rittenhouse, R. C.; Ornstein, R. L. *J. Am. Chem. Soc.* **1999**, *121*, 7279.
(8) Hong, S. B.; Raushel, F. M. *Biochemistry* **1999**, *38*, 1159.
(9) Caldwell, S. R.; Newcomb, J. R.; Schlecht, K. A.; Raushel, F. M. *Biochemistry* **1991**, *30*, 7438.

10.1021/ja000439r CCC: $20.00
Published on Web 01/12/2001

Scheme 1. Enzymatic Hydrolysis of Paraoxon

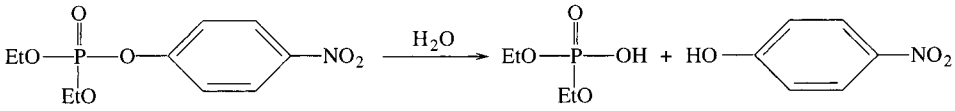

Scheme 2. Substrates Studied in This Paper: Paraoxon (left) and Sarin

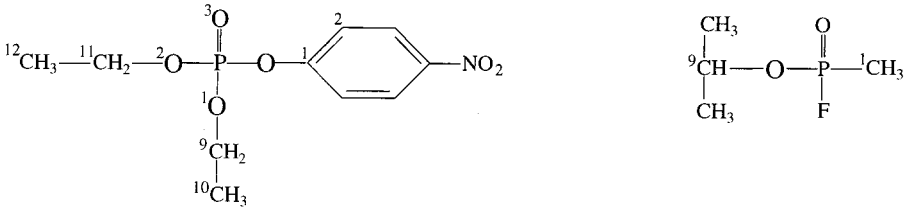

Scheme 3. A Schematic Representation of the PTE Active Site[a]

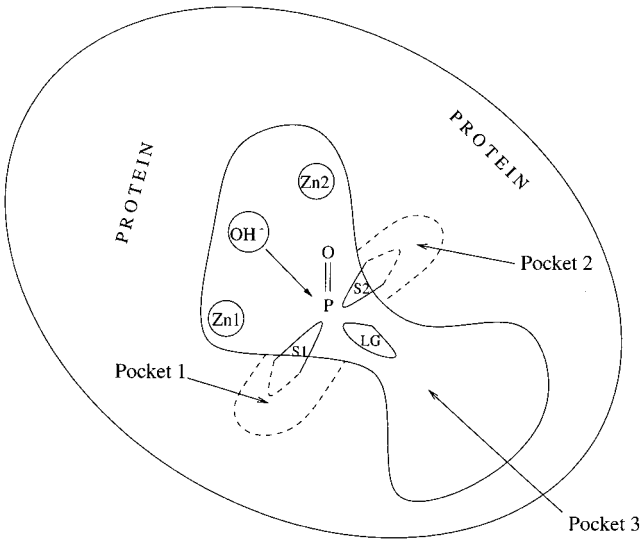

[a] It is composed of three pockets[8] where the substituents S1 and S2 on the phosphorus atom are positioned. Pocket 1 is mainly composed of His-257, Leu-271, Phe-306, and Met-317. Pocket 2 consists of Trp-131, Ile-106, Leu-303, Phe-306, His-57, and newly considered Gly-60. Pocket 3, suited for the leaving group, is roughly defined by Trp-131, Phe-132, Leu-271, Phe-306, and Tyr-309

be positioned on opposite sides of the plane formed by the three remaining atoms attached to the phosphorus. This arrangement, however, would not be achieved if, for example, the paraoxon were to be positioned like the inhibitor in the crystal structure. At the same time, the leaving group would not be able to leave in this case[18] as it would be buried in the hydrophobic pocket 1.

In addition, kinetic data obtained on a series of paraoxon analogues[8] show that hydrolysis is stereochemically dependent and sensitive to the relative size of the two alkyl or aryl substituents that must fit into the two hydrophobic pockets of the enzyme. This is consistent with previous stereochemical observations.[3]

Finally, the experimental observations[4] obtained for a series of diethyl-substituted phenyl phosphates and their sulfur analogues, with PTE substituted by various metals, clearly indicate that the substrate is strongly polarized by the metal ions. This indicates direct coordination of the phosphoryl oxygen, or sulfur atom, with one or both metal ions. This is, however, not consistent with the X-ray crystal structure data where the closest distance between the phosphoryl oxygen of the inhibitor and the zinc atom is 3.4 Å.

The above observations imply that the positioning of the substrate in the active site of the enzyme, as well as the flexibility of the active site, play important roles in the enzymatic process. As the enzymatic reaction is very fast, it is difficult to obtain direct experimental data (for example, an X-ray crystal structure) on the enzyme/substrate complex. We have therefore employed molecular dynamics (MD) simulations on solvated PTE−substrate complexes, as well as quantum mechanical calculations on a simplified model of the active site complexed with the substrates, to address the following questions: (i) does the structure of the active site change (relative to the X-ray structure) when the protein is immersed in a water bath and relaxed by MD; (ii) how is the substrate positioned in the active site of the relaxed protein; (iii) does the substrate orientation account for the experimentally observed strong polarization of the P═O bond; and (iv) how does the substrate interact with the protein?

Calculation Methods

MD simulations were carried out on subunit 2 of the PTE dimer,[5] using the SANDER module of AMBER 5.0[10] with the force field reported by Cornell et al.[11] Partial atomic charges for paraoxon, sarin, and the carbamylated Lys-169 were determined by using the restrained electrostatic potential (RESP) procedure.[11] The bond and rotational parameters of a carboxylate group were used for the carbamylated end of Lys-169, and the bond, angle, and rotational parameters involving the central phosphorus in the substrates were adapted from parameters available for the phosphate group of DNA or RNA. A nonbonded model was employed to treat the zinc ions. The net charges on the zinc ions determined by the quantum chemical calculations are significantly smaller than 2.0 (as described below). Thus, the net charges used on the zinc ions should be smaller than 2.0, if a bonded model is chosen for the zinc ions. However, the charge 2.0, which is frequently used in simulations,[7,12−14] was employed in our present MD simulations so as to be consistent with the nonbonded model. The van der Waals interaction parameters of zinc were developed by Stote and Karplus[12] to balance the use of charge 2.0 within the CHARMM force field; their nonbonded model was shown to give reasonable Zn^{2+}−water radial distribution, free energies of solvation, and plausible protein MD simu-

(10) Case, D. A.; Pearlman, D. A.; Caldwell, J. W.; T. E. Cheatham, I.; Ross, W. S.; Simmerling, C.; Darden, T.; Merz, K. M.; Stanton, R. V.; Cheng, A.; Vincent, J. J.; Crowley, M.; Ferguson, D. M.; Radmer, R.; Seibel, G. L.; Singh, U. S.; Weiner, P. K.; Kollman, P. A. *AMBER*, 5.0; University of California: San Francisco, 1997.

(11) Cornell, W. D.; Cieplak, P.; Bayly, C. I.; Gould, I. R.; Merz, K. M.; Ferguson, D. M.; Spellmeyer, D. C.; Fox, T.; Caldwell, J. W.; Kollman, P. A. *J. Am. Chem. Soc.* **1995**, *117*, 5179.

(12) Stote, R. H.; Karplus, M. *Proteins* **1995**, *23*, 12.

(13) Roxstrom, G.; Velazquez, I.; Paulino, M.; Tapia, O. *J. Phys. Chem. B* **1998**, *102*, 1828.

(14) Bordo, D.; Matak, D.; Djinovic-Carugo, K.; Rosano, C.; Pesce, A.; Bolognesi, M.; Stroppolo, M. E.; Falconi, M.; Battistoni, A.; Desideri, A. *J. Mol. Biol.* **1999**, *285*, 283.

lation results.[12] Using the AMBER force field, we previously obtained[7] good agreement with the experimentally observed Zn^{2+}−water radial distribution. Since the AMBER and CHARMM force fields are similar and since our current focus is on structure and not thermodynamics, we did not calculate free energies of solvation with the AMBER.

In the current work, seven 500-ps simulations were produced, five on the fully solvated protein and two on the gas-phase substrates, paraoxon and sarin. Initially, two simulations were carried out on the Zn-substituted PTE−paraoxon complex. The first (PAR1) started with the X-ray crystal structure of the Zn-substituted PTE complex replacing the inhibitor with the paraoxon substrate. The paraoxon was positioned similarly to the inhibitor and with the esteric oxygen attached to the nitrobenzyl group superimposed on the methylene carbon attached to the benzyl group of the inhibitor. In this position the leaving group of paraoxon is positioned in pocket 1 which is not suited for departure from the active site. The starting structure for the second trajectory (PAR2) was generated in the same way except that the substrate was rotated to place the nitrobenzyl group in pocket 3 (see Scheme 3). The substrate's ethoxy groups were positioned in pockets 1 and 2, respectively. The analysis of data generated by the above simulations shows that paraoxon may bind to PTE in either position.

It was predicted in the literature[8] that the sarin enantiomer $R_{p-}(+)$ should be a better substrate than $S_{p-}(-)$. We expected that simulations with $R_{p-}(+)$ would lead to the same findings as we have seen in previous data obtained for paraoxon, since the bulky substituent would be positioned in the same way as the nitrobenzyl group of paraoxon. Therefore, the $S_{p-}(-)$ enantiomer was chosen to test the placement of the bulky substituent in pocket 2 and still have the leaving group positioned appropriately. The first sarin simulation (SAR1) started with the X-ray crystal structure of the PTE complex, replacing the inhibitor by sarin in such a way that the P═O bonds were superimposed and the fluorine atom was superimposed on the benzyl methylene carbon of the inhibitor. This approach produced an orientation of the substrate in which the methyl group of sarin adopted a position in pocket 2 and the bulky $OCH(CH_3)_2$ group was positioned as the leaving group. The starting geometry for the second simulation (SAR2) was generated with sarin rotated about the P═O axis by 120°, putting the fluorine atom in the position of the leaving group. The methyl group was positioned in pocket 1 and the remaining bulky group in pocket 2. The final simulation (PTE) included only the solvated enzyme (no substrate). The starting geometry was generated from the X-ray structure with removal of the inhibitor.

A 2-fs time step was used in all simulations and the particle-mesh Ewald (PME) method[15] was employed. Each simulation started from the 2.1 Å resolution X-ray crystal structure[5] with the substrate positioned as described above. The all-atom model was neutralized by adding two chloride counterions and was immersed in a rectangular water box. The initial size of the box in all five cases was 77.0 × 76.0 × 71.0 $Å^3$ and it contained 10787, 10789, 10781, 10785, and 10833 TIP3P water molecules for the PAR1, PAR2, SAR1, SAR2, and PTE trajectories, respectively. The protein−solvent system was optimized prior to the simulation as follows. First, the protein was frozen and the solvent molecules with counterions were allowed to move during a 1000-step minimization and a 2-ps molecular dynamics run. Second, the side chains were allowed to relax by several subsequent minimizations during which decreasing force constants were put on the backbone atoms. After full relaxation, the system was slowly heated to 250 K in 10 ps and then to 300 K in 40 ps.

The simulations were initiated with a periodic boundary condition in the NPT ensemble at 300 K with Berendsen temperature coupling[16] and constant pressure (1 atm) with isotropic molecule-based scaling.[16] The SHAKE algorithm,[17] with a tolerance of 10^{-5}, was applied to fix all bonds containing a hydrogen atom, and the nonbond pair list was updated every 10 steps. The PAR1 trajectory was repeated at constant volume and constant pressure with no significant difference in RMSD;

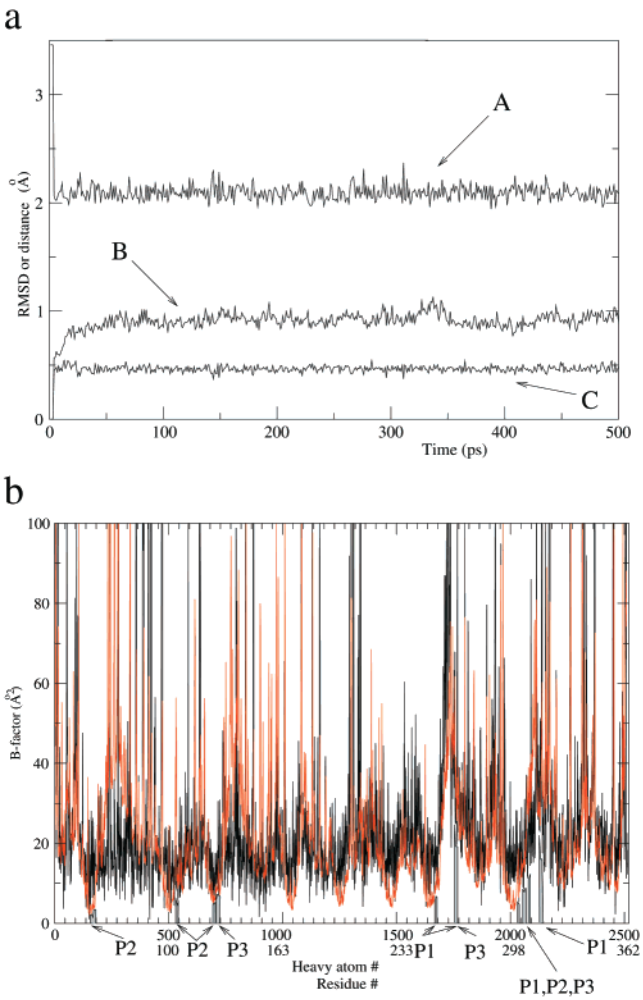

Figure 1. General characteristics of the PAR1 simulation: (a) distance between the less buried zinc atom and the phosphoryl oxygen of paraoxon (A), RMSD (heavy atoms) of the active site residues from the X-ray crystal structure (starting geometry) (B), and RMSD from the starting geometry calculated for a subset of atoms composed of both zinc atoms, oxygen of the hydroxide, phosphorus, and the phosphoryl oxygen (C); (b) B-factors obtained from the X-ray (black) and MD simulation (red, calculated from last 200 ps of the PAR1 trajectory).

for reasons of computational ease, all the other simulations were switched from constant pressure to constant volume after the density became balanced. The two gas-phase simulations (paraoxon-PAR, sarin-SAR) were carried out with the same parameters as stated above. The same starting orientations were used as in PAR1 and SAR1 trajectory for paraoxon and sarin, respectively. The *B*-factors were calculated as described in the literature[18] using the equation $B_i = (8\pi^2/3)R^2$, where B_i and R_i are the B-factor and RMSD of atom *i*, respectively.

Quantum chemical calculations were carried out by using the Gaussian94[19] and Gaussian98[20] programs on IBM SP2 and SGI Origin 200 multiprocessor computers. All the calculations employed a simplified active site model of the zinc substituted as described elsewhere.[7] In the simplified model, the carbamylated Lys 169 and Asp 267 residues are replaced by $NH_2CO_2^-$ and CHO_2^-, respectively, and the His 55, His 57, His 201, and His 230 residues are represented as NH_3 molecules.

(15) Essmann, U.; Perera, L.; Berkowitz, M. L.; Darden, T. A.; Lee, H.; Pedersen, L. G. *J. Chem. Phys.* **1995**, *98*, 10089.
(16) Berendsen, H. C.; Postma, J. P. M.; Gunsteren, W. F. v.; DiNola, A.; Haak, J. R. *J. Comput. Phys.* **1984**, *81*, 3684.
(17) Ryckaert, J. P.; Ciccotti, G.; Berendsen, H. C. *J. Comput. Phys.* **1977**, *23*, 327.
(18) Resat, H.; Mezei, M. *Biophys. J.* **1996**, *71*, 1179.
(19) Frisch, M. J.; Trucks, G. W.; Schlegel, H. B.; Gill, P. M. W.; Johnson, B. G.; Robb, M. A.; Cheeseman, J. R.; Keith, T.; Petersson, G. A.; Montgomery, J. A.; Raghavachari, K.; Al-Laham, M. A.; Zakrzewski, V. G.; Ortiz, J. V.; Foresman, J. B.; Cioslowski, J.; Stefanov, B. B.; Nanayakkara, A.; Challacombe, M.; Peng, C. Y.; Ayala, P. Y.; Chen, W.; Wong, M. W.; Andres, J. L.; Replogle, E. S.; Gomperts, R.; Martin, R. L.; Fox, D.; Binkley, J. S.; Defrees, D. J.; Baker, J.; Stewart, J. P.; Head-Gordon, M.; Gonzalez, C.; Pople, J. A. *Gaussian 94*; Gaussian, Inc.: Pittsburgh, PA, 1995.

Table 1. The Average Distances (in Å) between Zinc Atoms and Their Coordination Partners[a]

	MD trajectory				quantum mechanics	
distance	PAR1	PAR2	SAR1	SAR2	PAR	SAR
Zn1−O	2.01(0.04)	1.97(0.03)	1.97(0.04)	1.99(0.04)	1.96	1.97
Zn1−NE2_55	2.32(0.13)	2.22(0.09)	2.17(0.10)	2.30(0.10)	2.08	2.08
Zn1−NE2_57	2.32(0.10)	2.18(0.06)	2.21(0.07)	2.25(0.07)	2.09	2.09
Zn1−OZ1_169	2.00(0.04)	1.99(0.04)	2.02(0.05)	2.00(0.05)	2.08	2.07
Zn1−OD1_301	2.02(0.04)	1.99(0.04)	2.00(0.04)	2.00(0.04)	2.09	2.09
Zn2−O	1.98(0.04)	1.97(0.03)	1.95(0.04)	1.96(0.03)	1.96	1.98
Zn2−ND1_201	2.31(0.09)	2.32(0.09)	2.29(0.08)	2.32(0.09)	2.13	2.14
Zn2−NE2_230	2.26(0.08)	2.26(0.08)	2.25(0.07)	2.26(0.08)	2.10	2.09
Zn2−OZ2_169	1.98(0.04)	1.99(0.05)	1.99(0.04)	1.98(0.04)	2.01	2.02
Zn2−O3P	2.09(0.06)	2.08(0.06)	2.07(0.06)	2.08(0.06)	2.15	2.14
P−O	3.38(0.13)	4.09(0.14)	3.87(0.25)	3.75(0.18)	3.13	3.10
Zn1−Zn2	3.62(0.06)	3.62(0.06)	3.62(0.06)	3.62(0.06)	3.31	3.32

[a] O stands for the oxygen atom bridging the two zinc atoms, Zn1 and Zn2 for the respectively more and less buried zinc atom, P for the phosphorus atom of the substrate, and O3P for the phosphoryl oxygen doubly bonded to that phosphorus atom. Values were obtained by averaging snapshots taken after 200 ps until the end of each trajectory. The values in parentheses are the standard deviation.

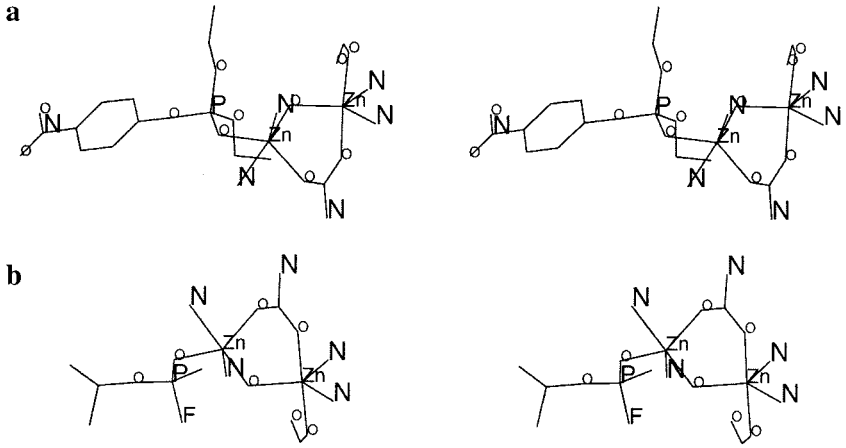

Figure 2. Stereoview of the PTE active site simplified model complexed with paraoxon (a) and sarin (b) as obtained by quantum mechanical calculations.

Previous ab initio and DFT calculations on the PTE active site models indicate that this simplified model is adequate for our purpose because all the optimized geometric parameters involving zinc ions do not significantly change when this simplified model is replaced by a more complete model.[7] Geometries of the PTE-substrate complex models were fully optimized by employing density functional theory (DFT) using Becke's three-parameter hybrid exchange functional and the Lee−Yang−Parr correlation functional (B3LYP)[21,22] with the 6-31G* basis set. The corresponding vibrational frequencies were evaluated at the optimized geometries to verify their true stability. Previous ab initio and DFT calculations[7] on the PTE active site models indicate that the geometries optimized at the HF/3-21G, HF/6-31G*, B3LYP/6-31G*, and MP2/6-31G* levels of theory are all consistent with each other and they are all very close to the corresponding parameters in the reported X-ray crystal structure.[5]

The graphics and molecular modeling were performed using Rasmol, Xfig, and Grace software.[23]

Results and Discussion

All of the MD trajectories became stable between 200 and 300 ps. This is illustrated for the PAR1 simulation in Figure 1 which shows RMSD of the MD simulation from the initial X-ray structure and X-ray *B*-factors. Generally there is very good agreement between the X-ray and MD data. There are only two portions of the protein where the values significantly differ; residues 65−87 (atom nos. 217−404) and residues 136−148 (atom nos. 768−874). Both are solvent exposed parts of the protein that are distant from the active site.

Position of the Substrate in the Active Site. The average values of distances between the zinc ions and the coordinated residues, the bridging ion, and the substrate are given in Table 1, together with the RMSD values. It is seen that the RMSD values are very small which indicates a well-defined minimum on the energy surface of the enzyme−substrate system. The geometry of the active site−substrate complex is also in good agreement with the quantum mechanics results (Table 1 and Figure 2). The only significant nonbonded internuclear distance differences between the MD and quantum mechanically optimized active site geometries are between the substrate phosphorus and the bridging hydroxide oxygen, and between the two zinc ions.

A comparison of the distances for the PAR1 and PAR2 trajectories implies that the first discrepancy could be ascribed

(20) Frisch, M. J.; Trucks, G. W.; Schlegel, H. B.; Scuseria, G. E.; Robb, M. A.; Cheeseman, J. R.; Zakrzewski, V. G.; Montgomery, J. A.; Stratmann, R. E.; Burant, J. C.; Dapprich, S.; Millam, J. M.; Daniels, A. D.; Kudin, K. N.; Strain, M. C.; Farkas, O.; Tomasi, J.; Barone, V.; Cossi, M.; Cammi, R.; Mennucci, B.; Pomelli, C.; Adamo, C.; Clifford, S.; Ochterski, J.; Petersson, G. A.; Ayala, P. Y.; Cui, Q.; Morokuma, K.; Malick, D. K.; Rabuck, A. D.; Raghavachari, K.; Foresman, J. B.; Cioslowski, J.; Ortiz, J. V.; Stefanov, B. B.; Liu, G.; Liashenko, A.; Piskorz, P.; Komaromi, I.; Gomperts, R.; Martin, R. L.; Fox, D. J.; Keith, T.; Al-Laham, M. A.; Peng, C. Y.; Nanayakkara, A.; Gonzalez, C.; Challacombe, M.; Gill, P. M. W.; Johnson, B.; Chen, W.; Wong, M. W.; Andres, J. L.; Gonzalez, A. C.; Head-Gordon, M.; Replogle, E. S.; Pople, J. A. *Gaussian 98*, revision A.6; Gaussian, Inc.: Pittsburgh, PA, 1998.

(21) Becke, A. D. *J. Chem. Phys.* **1993**, *98*, 5648.

(22) Lee, C.; Yang, W.; Parr, R. G. *Phys. Rev. B* **1988**, *37*, 785.

(23) Sayle, R. *Rasmol 2.5*; Sayle, R., Ed.; Glaxo Wellcome Research and Development: Stevange, Hertfordshire, UK, 1996.

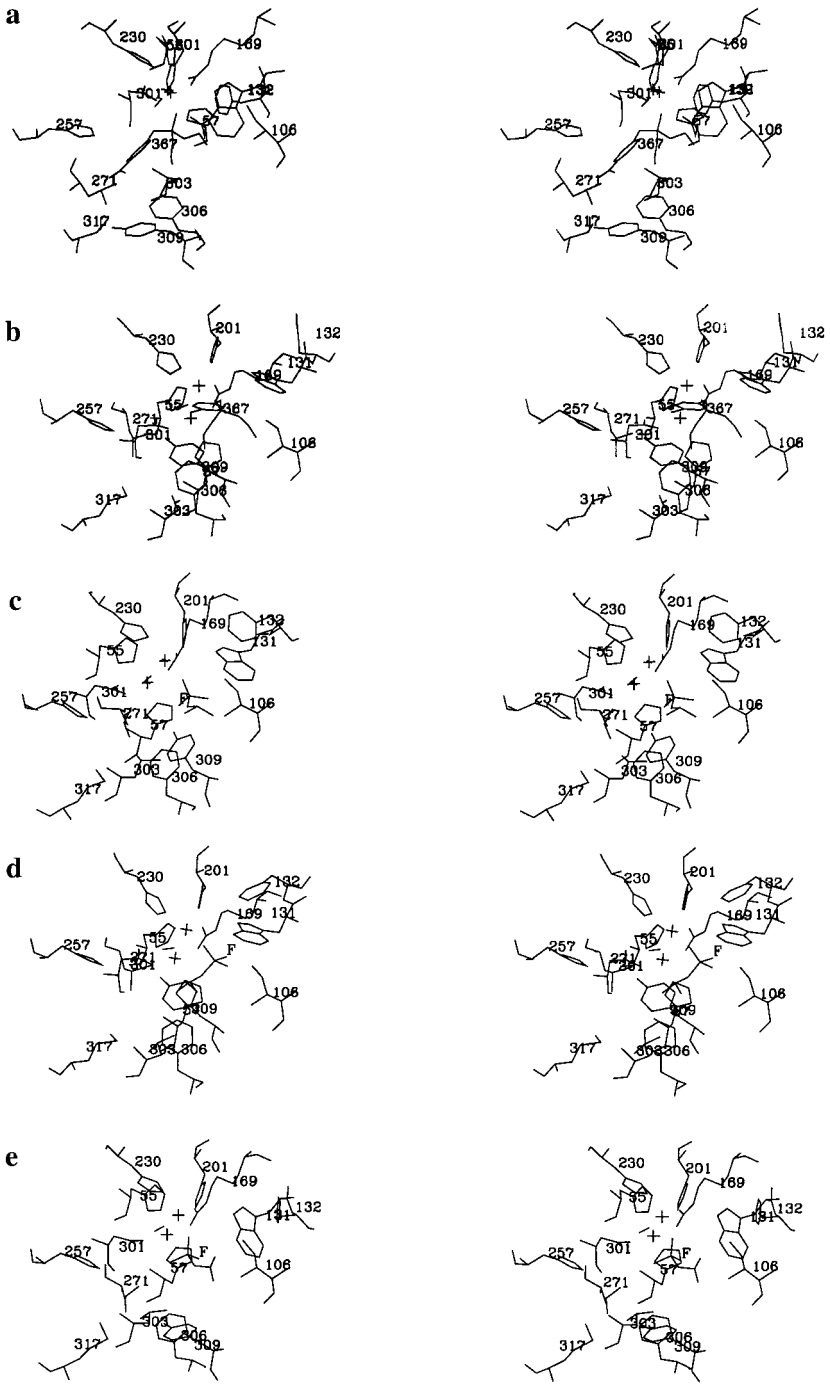

Figure 3. Stereoview of PTE active site−substrate complexes (zinc ions are represented by the crosses, the hydroxide by the black stick in close proximity to the zincs): average structures from the last 400 ps of PAR1 (a), PAR2 (b), and SAR2 (e) simulations, respectively; snapshot taken at the 200th (c) and 278th (d) ps of the SAR1 simulation. Paraoxon is labeled by 367 and sarin by F to show which substituent is the fluorine atom.

to the reduced model used in the quantum mechanical calculations. The second difference probably comes from the force field parameters. It is seen that the geometry of the complex around each of the zinc atoms is a significantly distorted trigonal bipyramid. The reason for the distortion is that the substituents are not equivalent and, maybe more importantly, the two zinc ions are bridged by the OH^- ion.

There is one substantial difference when one compares the X-ray structure with the active site geometry from the MD. All the simulations show that the substrate rotates slightly in the active site compared to the inhibitor position in the X-ray structure, and the phosphoryl oxygen of the substrate becomes strongly coordinated with the less buried zinc atom very early in the simulation (Figure 1). The same behavior is exhibited by the substrate analogue, diethyl 4-methylbenzylphosphonate.[24] This observation, together with the relatively stable distance of the phosphorus atom from the hydroxide oxygen (Figure 3, Table 1), implies that the key atoms of the substrate are very well positioned in the enzyme to allow the nucleophilic attack by the hydroxide that is the first step of the S_N2 mechanism. It is interesting that for the most appropriately positioned paraoxon (PAR2), which is the best substrate known for PTE, this distance is the largest in the set of simulations we show here. The representative structures obtained from each trajectory are shown in stereoview in Figure 3.

(24) Unpublished detailed results for the 500 ps trajectory on zinc substituted PTE with substrate analogue diethyl 4-methylbenzylphosphonate bound are described in ref 7.

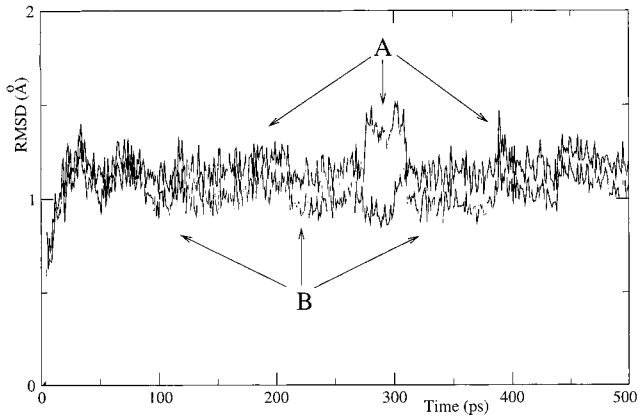

Figure 4. RMSD from the starting geometry calculated for only the active site residues (B) and for the active site residues and sarin (A).

To examine the polarization of the substrate caused by the positive charge on the less buried zinc ion, we performed two single-point energy calculations at the B3LYP/6-31G* level on paraoxon with the presence of a point charge representing the net charge on the zinc. In one calculation, the relative position of the point charge to paraoxon was the same as the relative position of the zinc to paraoxon in the optimized geometry of the PTE−paraoxon complex model in which the distance between the zinc and the phosphoryl oxygen is 2.159 Å. In the other calculation, the distance between the point charge and the phosphoryl oxygen was changed to 3.440 Å, the distance between the zinc and the phosphoryl oxygen in the reported X-ray crystal structure of the Zn-substituted PTE−inhibitor complex. The point charge used in the calculations was chosen as the net charge of the less buried zinc, +1.284, in the previously examined larger active site model of PTE (model 1L in ref 7 calculated at the HF/6-31G* level with the Merz−Singh−Kollman electrostatic potential fitting scheme). The energy decreases calculated for paraoxon, due to the presence of the point charge +1.284 at the distances 3.440 and 2.159 Å, are 11.3 and 45.1 kcal/mol, respectively. Correspondingly, the net atomic charges on the oxygen atom based on Mulliken population analysis are −0.575 (without the point charge), −0.654 (with the point charge at the distance 3.440 Å), and −0.772 (with the point charge at the distance 2.159 Å). Similarly, the charges on the phosphorus atom are +1.207 (without the point charge), +1.213 (with the point charge at the distance 3.440 Å), and +1.230 (with the point charge at the distance 2.159 Å). Thus, decreasing the distance between the point charge and the phosphoryl oxygen from 3.440 to 2.159 Å increases the energy lowering effect of the charge by about a factor of 4 and results in a much more strongly polarized P−O bond. The position of the substrate with respect to other residues of the active site is quite stable in the course of all but one of the simulations. This is deduced from the RMSD calculated for all residues of the active site and compared with the RMSD calculated for the same set of residues with the substrate included. However, it is not the case for the SAR1 run where the substrate is found to change position with respect to the active site residues (Figure 4). It is seen that while the RMSD calculated for all the active site residues remains unchanged (bottom curve), the RMSD calculated for the active site where the substrate is included (upper curve) exhibits a shift at around 300 ps. Both the original and the new positions are shown in Figure 3c,d. More detailed inspection of the SAR1 trajectory reveals that sarin rotates around the Zn−O axis in such a way that the distance between the phosphorus atom of sarin and the hydroxide oxygen becomes a little longer. The fluorine substituent, originally situated in pocket 1, moves closer to pocket 2. Simultaneously, the bulky substituent moves to pocket 1 and the methyl group moves to pocket 3, which is suited for the leaving group. The movement is accompanied by a conformational change around the P−O bond of sarin as clearly seen in Figure 6f (see below). Since fluorine is the leaving group in sarin, the new location is more favorable as fluorine and the hydroxide oxygen are now located more or less on opposite sides of the plane defined by the remaining three substituents on the phosphorus atom. However, the new location of the substituents in the pockets is not fully stabilized and the substrate returns after about 40 ps to its original position (see Figure 4). But the new sarin conformation is kept (see Figure 6f below). Although the position temporarily adopted is not ideal for hydrolytic cleavage, the movement implies that for chiral substrates with small substituents, the difference in activity between enantiomers may not be large. This observation is in good agreement with the experimental data.[8]

Flexibility of the Active Site. The key advantage of molecular dynamics is that it gives us a chance to follow the dynamics of a system within a certain time scale. Although the time scale is still generally limited to the submicrosecond range, even this period of time may provide substantial insight into processes that occur in biological systems such as proteins. We have analyzed the simulation trajectories and have followed several geometry parameters that characterize the PTE−substrate complex. Selected characteristics are plotted in Figures 5 and 6.

The first thing we were interested in was the question of whether the active site of the enzyme will remain unchanged when the enzyme is immersed in a water bath and allowed to relax. We were especially interested in pocket 3, which is probably the gateway where the substrate enters the enzyme and where the products of the enzymatic reaction leave the protein.[5,8] We have measured the distance between two side chains (Phe-132 and Leu-271),that appear to form the entrance to the active site, expressed by the separation between the CE2 carbon of Phe-132 and the CD1 carbon of Leu-271. The results are shown in Figure 5. In the absence of a substrate, the gateway opens to about 14 Å, while the original X-ray distance is about 8 Å (Figure 5a). The opening is flexible and exhibits large changes with respect to the X-ray structure ranging from 1 to 10 Å. Figure 5b shows that the gateway opening is dependent on the substrate or, more specifically, on the substituent that is positioned in pocket 3. The opening is relatively large when the substituent is bulky, like the benzene ring in the case of the PAR2 trajectory. The opening is mainly caused by a crankshaft movement of the Phe-132 residue (Figure 5e). The effect is clearly seen when comparing the X-ray structure (Figure 5c) and the MD relaxed (Figure 5d) structure of the enzyme. Comparison of the X-ray and MD *B*-factors reveals that there is no substantial change in the flexibility of the gateway after it opens. Both the experimental and MD *B*-factors are very low (less than 20 $Å^2$) for the backbone part of Leu-132 and increase to about 40 $Å^2$ for the benzene ring atoms (see Figure 1b, atom nos. 735−745).

Although a logical conclusion would be that a larger substituent should require a larger opening, it is not always so. For example, the gateway is relatively closed when a bulky $OCH(CH_3)_2$ substituent is positioned there (Figure 5b, bottom curve). The opening of the gateway in pocket 3 is also observed for the two remaining trajectories where the distances are found to be between the values shown in Figure 5b.

Conformational changes in the substrates may be followed by tracking key dihedral angles over the course of the simula-

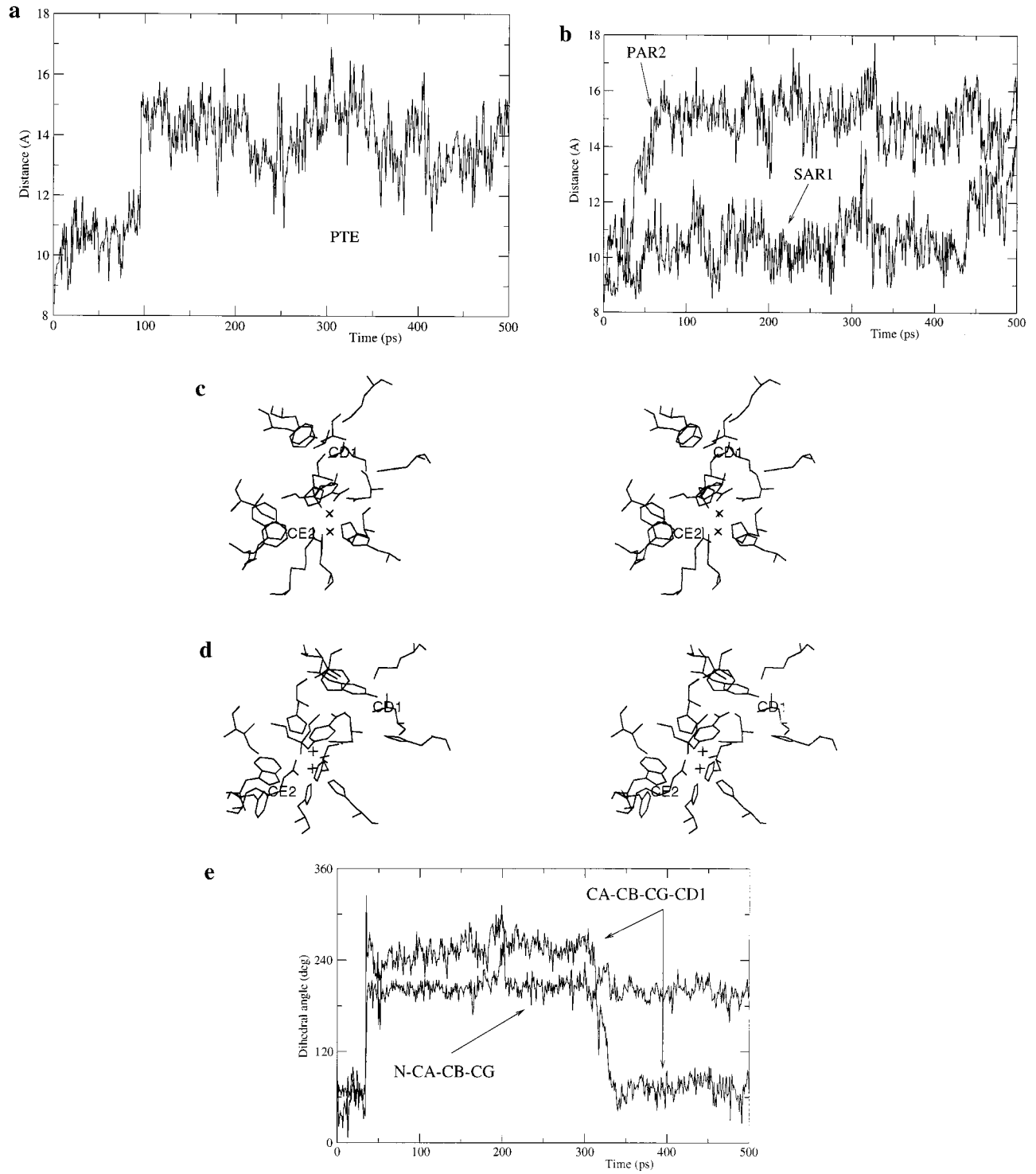

Figure 5. Distance between the CD1 carbon of Leu-271 and the CE2 carbon of Phe-132 calculated for several trajectories (a, b). Stereoview of the zinc-substituted PTE active site with paraoxon positioned as described in the Method section for the PAR2 trajectory. X-ray structure of the enzyme with paraoxon superimposed (c); the snapshot taken at 327 ps when the opening is the most significant (d); and history of selected Phe-132 dihedral angles (e).

tions as seen in Figure 6. Different behaviors were observed for different substrate substituents and for different active site pockets.

The dihedral angle analysis suggests that pocket 1 is the most accommodating, exhibiting very high flexibility (see *B*-factors, Figure 1b). It appears spacious enough to fit a bulky substituent and it may allow for conformational movement of such substituents as the nitrobenzyl group of paraoxon in the PAR1 simulation (Figure 6a) or one of the terminal ethyl groups in the PAR2 simulation (Figure 6d). The time course of the curves shows that the residues of the pocket assist in the conformational movement. However, when a smaller substituent is present, as in the case of the ethoxy group (Figure 6b), the contacts are different and the curve is more flat. Behavior of the same group is completely different in pocket 2 during the PAR1 simulation (Figure 6c), indicating that pocket 2 may be smaller.

Pocket 3 is expected to be the most elastic because of the flexible gateway discussed above. This is confirmed by our data. Conformational flexibility is observed for the nitrobenzyl substituent in the PAR2 simulation (Figure 6a), for one of the

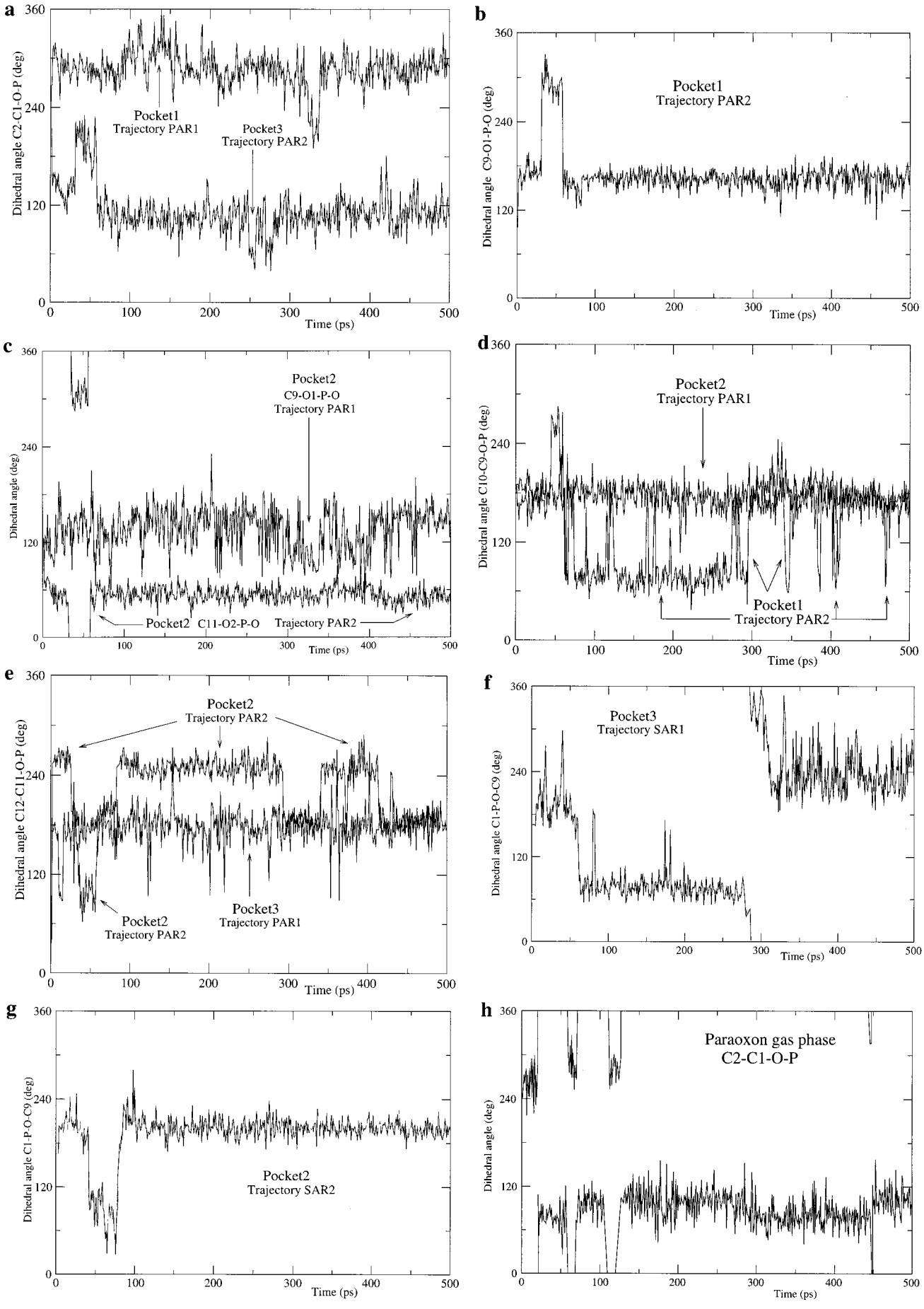
a
Dihedral angle C2-C1-O-P (deg)
Pocket1
Trajectory PAR1
Pocket3
Trajectory PAR2
Time (ps)
b
Dihedral angle C9-O1-P-O (deg)
Pocket1
Trajectory PAR2
Time (ps)
c
Dihedral angle (deg)
Pocket2
C9-O1-P-O
Trajectory PAR1
Pocket2 C11-O2-P-O Trajectory PAR2
Time (ps)
d
Dihedral angle C10-C9-O-P (deg)
Pocket2
Trajectory PAR1
Pocket1
Trajectory PAR2
Time (ps)
e
Dihedral angle C12-C11-O-P (deg)
Pocket2
Trajectory PAR2
Pocket2
Trajectory PAR2
Pocket3
Trajectory PAR1
Time (ps)
f
Dihedral angle C1-P-O-C9 (deg)
Pocket3
Trajectory SAR1
Time (ps)
g
Dihedral angle C1-P-O-C9 (deg)
Pocket2
Trajectory SAR2
Time (ps)
h
Dihedral angle (deg)
Paraoxon gas phase
C2-C1-O-P
Time (ps)

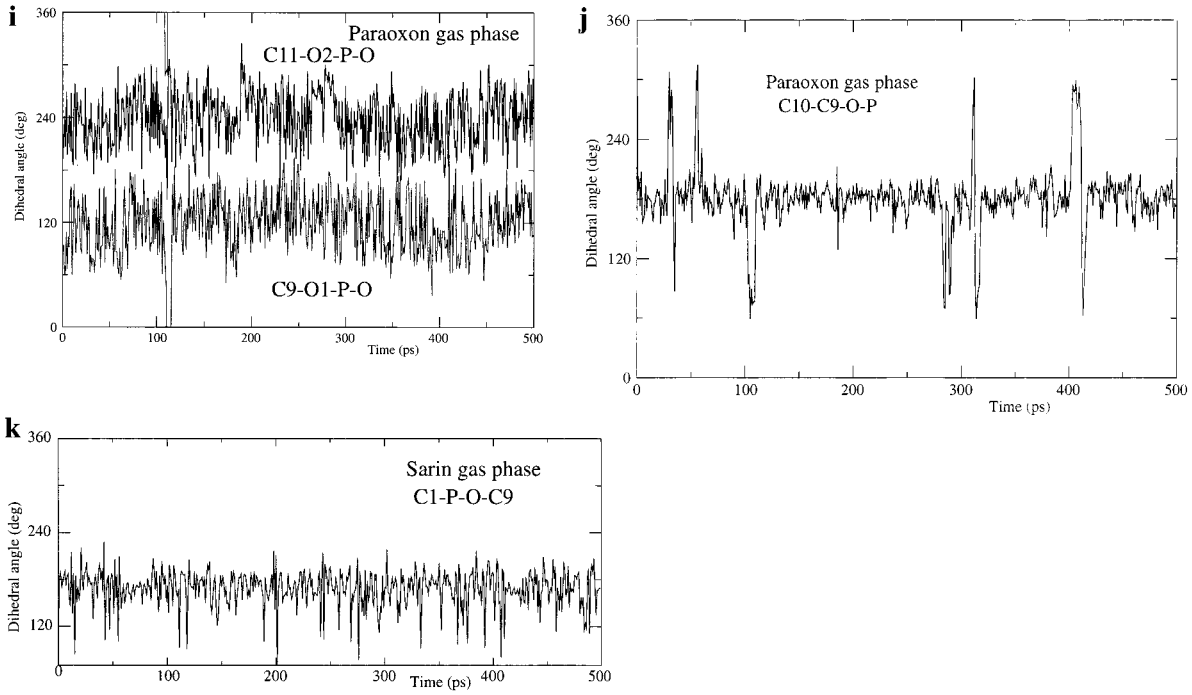

Figure 6. History of selected dihedral angles for substrate substituents localized in different active site pockets and obtained from different trajectories.

terminal ethyl groups in the PAR1 simulation (Figure 6e), as well as for the bulky $OCH(CH_3)_2$ group of sarin in the SAR1 simulation (Figure 6f). Flexibility of the pocket is seen also from *B*-factors (Figure 1b) which show that not all the residues forming pocket 3 exhibit the same flexibility.

The most complicated behavior is observed for pocket 2, which is the smallest and the least flexible. Presumably, it is the one most responsible for the stereoselectivity of PTE.[8] The bulky $OCH(CH_3)_2$ group does not move (after the initial repositioning during the equilibration protocol) within pocket 2 (Figure 6g) while the same group moves much more frequently when placed in pocket 3 (Figure 6f, especially the second part of the trajectory). The data in Figure 6e show that one of the paraoxon's terminal ethyl groups exhibits several conformational changes in pocket 2, while pocket 3 allows for larger conformational movement just within one basic conformation. Probably the most interesting data on pocket 2 are plotted in Figure 6c, which shows conformational behavior of the same group in pocket 2 for different simulations or, in other words, for different occupations of the remaining pockets. It is clearly seen that while the ethoxy group of paraoxon is quite flexible in pocket 2 during the PAR1 simulation, it is much less flexible in the same pocket during the PAR2 simulation. This indicates that either pocket 2 is flexible and its opening or closing is related to the occupation of pocket 3 or the position of the ethoxy group in pocket 2 is different for the two simulations. *B*-factors shown in Figure 1b support the latter statement, revealing that pocket 2 belongs to the most rigid parts of the protein. This is in agreement with the observed absence of dihedral angle movement correlations between pockets 2 and 3.

Comparison of either substrate dihedral angle histories in the gas phase versus the entire system simulations (Figure 6) indicates how the conformational behavior of the substrate within the protein is influenced by the protein. In some cases, the dihedral movement within a pocket is almost the same as it is in a vacuum, for example, the dihedral C10−C9−O−P in PAR1 simulation (Figure 6d,j). On the other hand, the dihedral movements may be substantially different in the gas phase and within the protein as observed for both the paraoxon (for example, dihedrals C12−C11−O−P (Figure 6e) and C10−C9−O−P (Figure 6d,j) in PAR2 simulation) and sarin (Figure 6f,g,h) substrates.

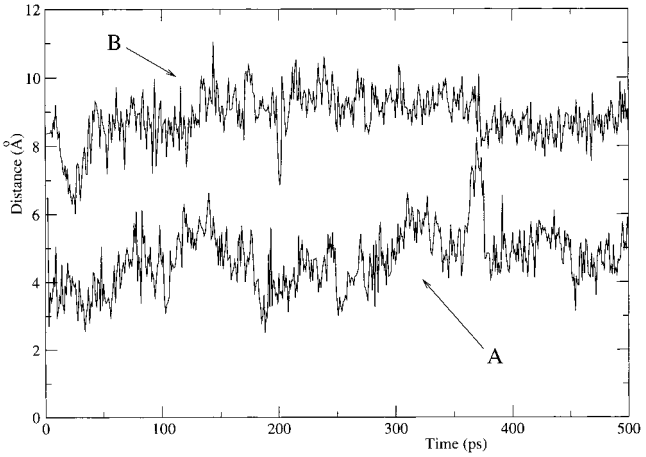

Figure 7. Distance between the hydroxyl hydrogen of Tyr-309 and one of the oxygen atoms of paraoxon's nitro group (A) and the fluorine atom of sarin (B), respectively.

We have also performed careful analysis of hydrogen bonding between the substrate and the protein. This was done for all applicable trajectories and no significant hydrogen bonding was found, implying that the above-discussed interactions between the substrate and the protein are fully based on van der Waals contacts and steric repulsions.

Hypothesis on the Role of Tyr-309 Residue. Kinetic studies have shown that the rate-limiting step of enzymatic hydrolysis may involve a conformational change or diffusion-controlled dissociation.[9] Under these conditions, the departure of the leaving group from pocket 3 may be rate limiting. An interaction that possibly assists the leaving group, as it exits from hydrophobic pocket 3, is hydrogen bonding between one or both oxygen atoms of the NO_2 group of paraoxon and hydroxyl group of Tyr-309 (see Figures 3b and 5d). This interaction is much stronger for paraoxon than the analogous interaction with sarin (Figure 7).

Site-directed mutagenesis of Tyr-309 (to, for example, Phe), as well as a hydrolytic rate determination for a paraoxon substitute without the nitro group, could test the validity of this hypothesis.

Conclusions

The results obtained from the molecular dynamics simulations show that multiple orientations of paraoxon in the active site of zinc-substituted PTE are possible. The same applies for sarin where two orientations of the $S_p(-)$ enantiomer, which is expected to be less favorable for hydrolysis, were examined. Molecular dynamics and quantum chemical data indicate that PTE substrates can adopt alternative positions in the active site than what is observed for the substrate analogue in the X-ray crystal data. The phosphoryl oxygen becomes strongly coordinated to the less buried zinc cation, which allows for strong polarization of the reaction center of the substrate. These results indicate that the enzymatic hydrolysis occurs as a multistep process, in which formation of the substrate−protein complex is the first step.

There are conformational changes that occur throughout the active site region of PTE when the enzyme is immersed in the water bath and relaxed by MD. The most remarkable change is the opening of the gateway in pocket 3 where the leaving group is expected. The enzyme's gateway opens with and without substrate being present in the active site. The size of the opening is dependent on the substrate and may range from 11 to 18 Å. Different conformational behaviors are observed for the same substrate substituents within different pockets, for different simulations, as well as in the gas phase. This shows that the active site pockets generally contribute to the substrate binding. Detailed analysis of all trajectories reveals that this contribution in not based on hydrogen bonding. The computational results indicate that the key substrate−protein interaction occurs between the less buried zinc ion and the phosphoryl oxygen of the substrate. The *B*-factors obtained from X-ray and MD indicate that the portions of the protein that form pocket 2 are relatively rigid, while pockets 1 and 3 are much more flexible.

The preliminary theoretical data presented here are in good agreement with previous experimental observations and suggest an important inherent role of dynamic fluctuations contributing to specificity and the kinetic properties of PTE. MD studies of PTE mutants, with altered experimental specificity and/or kinetics, can test the importance of the trends noted above.

Acknowledgment. This work was supported by the National Security Division and Laboratory Directed Research and Development Program (LDRD) at Pacific Northwest National Laboratory (RLO). Pacific Northwest National Laboratory is a multiprogram national laboratory operated for the U.S. Department of Energy by Battelle Memorial Institute under contract DE-AC06-76RLO 1830. J.K. is a visiting professor from Masaryk University, Brno, The Czech Republic, C.G.Z. is a senior visiting scientist from Columbia University, and R.C.R. is a visiting professor from Walla Walla College.

JA000439R